Optimized Wideband Beamforming for mm-wave Communication Systems with Intelligent Reflecting Surfaces

Hiba A. Alsawaf, and Saad Ahmed Ayoob

Original scientific article

***Abstract*—Millimeter wave-based intelligent reflecting surface communications represent a promising technology enabling 6G networks. However, taking advantage of the bandwidth of millimeter wave and the characteristics of IRS leads to the problem of beam splitting, which makes the precise steering of the resulting beams at all frequencies complicated, resulting in large losses in array gain. This paper investigated the effect of millimeter wave beam splitting IRS systems and developed an IRS structure based on the sub-surface of its elements. The basic idea is to introduce time delay (TD) and phase shift units into the IRS elements to perform common phase and pre-delay modulation instead of traditional phase shift. Therefore, a wideband phase shift design is proposed, and delay precoding compensates for the losses in array gain due to beam splitting. Large antennas are used in the base station, resulting in double beam splitting. An analysis of the effect of the double beam splitting on array gain was presented, along with some solutions aimed at improving the performance of phase conditioning and delay coding in the base station and IRS. The simulation results show that the proposed design, which is based on phase shift and TD, effectively overcomes the challenge of beam splitting. The proposed design demonstrated a gain improvement of 94.5% compared to the conventional approach. The results showed that the use of phase shift TD phase shift (PTDP) resulted in a 54% increase in data rate compared to the conventional design in the beam splitting case at IRS. The use of only two-bit phase shifters in the proposed PTDP is sufficient for near-optimal performance of the system's ability to focus the signal in the desired direction through the precoding technique, through which the losses caused by beam splitting can be compensated. As observed by comparing the proposed PTDP-based wideband precoding design with the conventional design, the results prove that the proposed design is capable of compensating for the array gain loss resulting from the double beam splitting effect occurring at both BS and IRS.**

***Index terms*—Intelligent Reflecting Surface (IRS), mm-wave, beam split and phase shift.**

I. Introduction

Millimeter waves are the backbone of 5G and 6G wireless communication systems, thanks to their ability to exploit vast, unused frequency bands [1, 2].

Manuscript received October 18, 2024; revised November 20, 2024. Date of publication December 18, 2024. Date of current version December 18, 2024. The associate editor prof. Andrej Hrovat has been coordinating the review of this manuscript and approved it for publication.

H. A. Alsawaf is with the Electronics Engineering College, Ninevah University, Mosul, Iraq, and she is a PhD student in the College of Engineering, University of Mosul (email: hiba.hmdoon@ uoninevah.edu.iq).

S. A. Ayoob is with the College of Engineering, University of Mosul, Mosul, Iraq (email: sa_ah_ay@uomosul.edu.iq).

Digital Object Identifier (DOI): 10.24138/jcomss-2024-0090

Despite the great advantages of their high bandwidth, millimetre waves face great challenges in achieving wide coverage in real environments due to high propagation losses and the influence of obstacles in the environment [3, 4]. Compared to frequencies below 6 GHz, millimetre waves (mm-Wave) are more susceptible to blockage due to their higher directivity. Previously, the coordinated multipoint (CoMP) technique was used to address signal weakness caused by long distance, attenuation or interference between multiple beams [5, 6]. Currently, the intelligent reflecting surface (IRS) technique is used to address these problems [7]. IRSs are a promising and cost-effective solution. IRS is an intelligent surface used to modify the phase of the radio waves reflected from it, allowing control of the radiation direction [8]. Therefore, the application of IRS in millimetre wave communications makes it an ideal technology for 5G and beyond systems [9, 10]. IRS technology has aroused great interest recently, with current research focusing on aspects such as precoder design [11, 12], channel estimation [13, 14], and architectural design [15], with a main focus on narrowband applications. For example, RIS technology has been successfully applied in various communications systems to improve the quality of the received signal to the user [11]. The block coordinate descent algorithm was adopted as a tool to improve the system performance by adjusting the parameters in both the base station and the RIS, which increased the weighted sum rate [16].

Much research has focused on studying the use of RIS technology in broadband communications systems, especially in the millimetre wave bands [17-21]. The researchers show that hybrid relay networks supported by intelligent reflecting surfaces, especially when using machine learning algorithms, achieve good performance in millimetre wave systems [22]. In millimetre wave systems that use large, intelligent reflecting surfaces, the use of conventional beam generation methods results in the beam being scattered in multiple directions at different frequencies, which increases the problem of beam splitting, which is more severe in this frequency range than beam squint [19, 23-27]. The paper [19] focused on addressing the beam-squinting problem in millimetre-wave communications-aided RIS. The paper [28] reviewed the potential of remote sensing systems to revolutionize millimetre wave communication and sensing systems, focusing on studying the behaviour of beam splitting and then analyzing the factors affecting system performance.

The study [29] presented solutions to the beam splitting problem in terahertz communication systems by proposing two

designs of simultaneous transmit-receive intelligent reconfigurable reflective surface (STAR-RIS).

This paper has proposed network performance improvements over mmWave environments by developing precoding and RIS techniques. Emphasis was placed on solving channel interference problems and extending RIS use in wide bands. These solutions therefore mark a significant development in overcoming the challenges to mmWave signals compared to earlier studies.

The main contributions of this paper are:

1. A reduction in the effects of beam splitting in intelligent, reflecting surfaces (IRS). An IRS design based on sub-layers with a finite number of TD units is proposed. Each element of the sub-array consists of a cascaded arrangement of two-phase converters and a common T.D. unit. The arriving signal is sequentially processed by these components, passing through phase shift 1, the TD unit, and phase shift 2. This design enables switching from conventional narrowband preceding based on the phase to wideband preceding that combines phase and delay, achieving a better balance between data rate and cost of the device.
2. Frequency-dependent wideband precoding is designed based on the proposed surface structure, where the phases of the first layer of the sub-array are controlled to generate constructively interfering signals in the receiving elements, improving the quality of the received signal. The second layer is responsible for steering the beam toward the desired receiver at the carrier frequency. The common TD unit aligns the generated beams to the intended physical direction across all subcarriers.
3. Large antenna arrays at the base station, where the effect of double beam splitting becomes critical, have also been studied. Beams originating from the base station take different paths at different subcarriers and the beams impacted and reflected from the base station are split into separate directions. The gain of the array was studied under line-of-sight dominance conditions, and the wide-range precoding design of the RIS and the base station was separated without loss of optimum solution.

The remaining portions of this paper are arranged as follows: A thorough model of the signal and system is presented in section II. The impact of beam splitting on the IRS is analyzed in section III, while section IV presents the proposed IRS structure design and the analysis of this design. Section V includes Solving the effect of double beam splitting. The results and simulation have been explained in section VI, while section VII concludes the paper.

Notations:

A^T: A new matrix was obtained by replacing the rows of matrix A with its columns.

A^H: A new matrix is obtained by taking the conjugate of the elements in A^T.

|a|: the length of vector a.

E[Z]: The random variable Z's anticipated average value.

$U(a,b)$ A probability distribution where all values between a and b are equally likely.

$\otimes$: A special multiplication operation between two matrices is called Kronecker multiplication.

$\odot$: Another special multiplication operation between two matrices is called Hadamard multiplication.

$diag(a)$: Is the diagonal matrix.

$blkdiag(a)$: Represents the block diagonal matrix.

II. System and Signal Model

This paper dealt with a millimetre wave communication system with the assistance of the IRS, as shown in Figure (1). The base station (BS) consists of a uniform linear array (ULA) with B antennas while the assistance of the IRS was used to transmit a signal to a single user; however, the model can also be applied to more than one user, if one user is taken for easy system analysis. $N = N_1 N_2$ It is the division of the IRS's N-element uniform planner array (UPA) into N_1 and N_2. Q subcarriers were used in orthogonal frequency division multiplexing (OFDM) to modulate user signals and reduce the wideband channel dispersion. The IRS was placed in the x-y plane. Where the BS was placed at (0,0), the IRS was at (0,25), and the user's location was (25,25).

The received signal at the q^{th} subscriber is given using the following equation [19]:

$$Y_q = (v_q^T \psi G_q + \underbrace{H_q}_{Blocked})X_q + \eta_q$$

$$Y_q = V_q^T \psi G_q X_q + \eta_q \quad (1)$$

where H_q: the direct channel between the base station and the user that is blocked, V_q^T: the channel between IRS and User [23]

$$V_q^T = \left[V_{q,1}, V_{q,2}, \ldots\ldots, V_{q,N}\right] \in \mathbb{C}^{1\times N}$$

$$\psi = diag(\theta) = diag\left(ie^{j\theta_1}, ie^{j\theta_2}, \ldots\ldots, ie^{j\theta_N}\right) \quad (2)$$

where ψ: The reflection coefficient of IRS, $i = 1$ a constant reflection amplitude assumed at the IRS [8, 30],$G_q \in \mathbb{C}^{N\times B}$presents the BS-IRS channel, $X_q = wr_q \in \mathbb{C}^{B\times 1}$ the transmitted signal at the base station, $w \in \mathbb{C}^{B\times 1}$is the precoding vector, $r_q \in \mathbb{C}$ is the transmitted data at the q^{th} subcarrier, which satisfies $\mathbb{E}[|r|^2] = 1$, r_q: it represented the Additive White Gaussian Noise (AWGN) with variance σ^2 and mean = 0 [31].

The reflecting surface is positioned to maintain a direct line of sight [32]. Therefore, the channel between BS and IRS is defined as [33-35]:

$$G_q = g_1(f_q, d_a)e^{-j2\pi f_q t_1}k(f_q, \alpha_1, \beta_1)\, b^H(f_q, \emptyset) \quad (3)$$

where $t_1 \in \mathcal{R}^+$ Represented the path delay, $g_1(f_q, d_a) \in \mathbb{C}$ denoted the path gain between the BS and IRS.

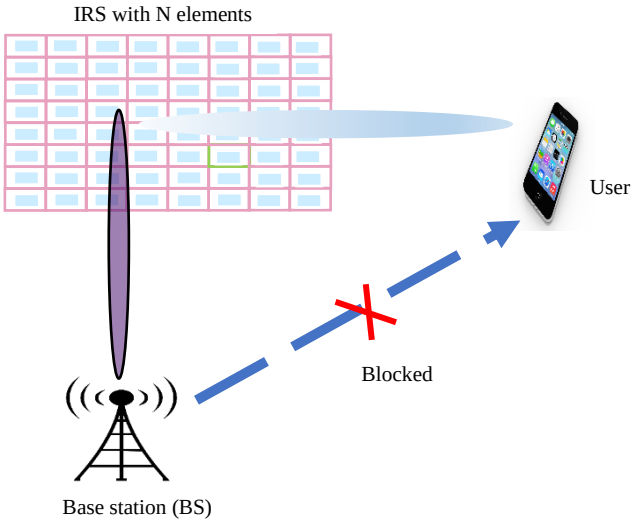

Fig. 1. The IRS-assisted mm-wave communications system

The q^{th}subcarrier frequency for $\forall\, q = 1, \ldots, Q$ is defined as [19, 36]:

$$f_q = f_c + \frac{f_s}{Q}\left(q - 1 - \frac{Q-1}{2}\right) \tag{4}$$

where f_c and f_s are the carrier frequency and bandwidth, the spacing between the IRS elements = $\frac{\lambda}{2} = \frac{c}{2f_c}$, as well as the spacing of the antenna of BS is set $\frac{\lambda}{2}$, c : represented the light speed.

The elevation angle α_1 and azimuth angle β_1 represent the direction from which the signal arrives at the IRS. The transmission angle of the base station is denoted ($\emptyset$). The following conditions constrain these angles: $\alpha \in U\left(0, \frac{\pi}{2}\right)$, $\beta \in U(-\pi, \pi)$and $\emptyset \in U\left(-\frac{\pi}{2}, \frac{\pi}{2}\right)$. The path gain between the BS and IRS is given by [33]:

$$g_1(f_q, d_a) = \frac{c}{4\pi f_q d_a} e^{\frac{-\tau(f_q)d_a}{2}} \tag{5}$$

where d_a It is the distance from BS to IRS, while $\tau(f_q)$ Representing the factor of medium absorption.

$k(f_q, \alpha_1, \beta_1)$ Is the IRS steering vector that is defined as [37, 38]:

$$k(f_q, \alpha_1, \beta_1) = \frac{1}{\sqrt{N}}\left[1, \ldots., e^{\frac{j2\pi f_q}{c}(N_1-1)dsin\alpha_1 cos\beta_1}\right]^T \otimes \left[1, \ldots., e^{\frac{j2\pi f_q}{c}(N_2-1)dsin\alpha_1 sin\beta_1}\right]^T \tag{6}$$

$b(f_q, \emptyset)$ is the base station steering vector, which is expressed as [39] :

$$b(f_q, \emptyset) = \frac{1}{\sqrt{B}}\left[1, \ldots., e^{\frac{j2\pi f_q}{c}(B-1)dsin\emptyset}\right]^T \tag{7}$$

In the same way, the channel between IRS and U is defined [40]:

$$V_q = g_2(f_q, d_b)\, e^{-j2\pi f_q t_2} k(f_q, \alpha_2, \beta_2) \tag{8}$$

where $t_2 \in \mathcal{R}^+$ represented the path delay, $g_2(f_q, d_b) \in \mathbb{C}$ denoted IRS-U channel's path gain, α_2 and β_2 the Angle of Departure's (AoD) azimuth and elevation angles $g_2(f_q, d_b)$ can be given [28]:

$$g_2(f_q, d_b) = \frac{c}{4\pi f_q d_b} e^{\frac{-\tau(f_q)d_b}{2}} \tag{9}$$

where d_b: The distance between the IRS and the user. The array gain at the q[th] subcarrier is expressed in terms of the system model [29]:

$$\begin{aligned}\mathbb{G}(f_q) &= \left|V_q^T \psi\, G_q w\right| \\ &= \left|g_1(f_q, d_a) g_2(f_q, d_b) e^{-j2\pi(t_1+t_2)f_q}\right|. \\ &\left|k^T(f_q, \alpha_2, \beta_2).\psi.k(f_q, \alpha_1, \beta_1) b^H(f_q, \emptyset) w\right|\end{aligned} \tag{10}$$

III. Analysis of Beam Splitting

The effect of beam splitting and array gain analysis on IRS was considered. Depending on equation (10), the IRS's normalized array gain at q[th] subcarrier was defined as [23, 29]:

$$\begin{aligned}\mathbb{G}_{RIS}(f_q) &= \left|k^T(f_q, \alpha_2, \beta_2)\psi\, k(f_q, \alpha_1, \beta_1) b^H(f_q, \emptyset)\right| \\ \mathbb{G}_{RIS}(f_q) &= \frac{1}{N}\left|\sum_{n_1=0}^{N_1-1}\sum_{n_2=0}^{N_2-1} e^{j\pi m[n_1(a_1+a_2)+n_2(\vartheta_1+\vartheta_2)]}\right|. \\ & e^{j\theta_\ell}\end{aligned} \tag{11}$$

where,$\ell = N_2 n_1 + n_2 + 1$, $a_1 = sin\alpha_1 cos\beta_1$,$\vartheta_1 = sin\alpha_1 sin\beta_1$, $a_2 = sin\alpha_2 cos\beta_2$, $\vartheta_2 = sin\alpha_2 sin\beta_2$,$N = N_1 N_2$,$m = \frac{f_q}{f_c}$ represented the relative frequency. The vector of beamforming for the IRS was determined using the carrier frequency of the transmitted signal as [29]:

$$\theta_\ell = -\pi[n_1(a_1 + a_2) + n_2(\vartheta_1 + \vartheta_2)] \tag{12}$$

It should be noted that the $g_1(f_q, d_a)$ and $g_2(f_q, d_b)$ is unaffected, the normalized array gain $\left(\mathbb{G}_{RIS}(f_q)\right)$. Equation (11) can be expressed more concisely as [23, 29]:

$$\mathbb{G}_{RIS}(f_q) = \frac{1}{N}\left|\sum_{n_1=0}^{N_1-1}\sum_{n_2=0}^{N_2-1} e^{j\pi(m-1)[n_1(a_1+a_2)+n_2(\vartheta_1+\vartheta_2)]}\right| \tag{13}$$

$$\mathbb{G}_{RIS}(f_q) \overset{(i)}{=} \mathbb{F}_{N_1}\left((m-1)(a_1+a_2)\right) \mathbb{F}_{N_2}\left((m-1)(\vartheta_1+\vartheta_2)\right) \tag{14}$$

where (i) comes from $\sum_{n=0}^{N-1} e^{jn\pi x} = \frac{sin\frac{N\pi x}{2}}{sin\frac{\pi x}{2}} e^{\frac{-j\pi(N-1)x}{2}}$ and $\mathbb{F}_N = \frac{sin\frac{N\pi x}{2}}{Nsin\frac{\pi x}{2}}$ is the Dirichlet Sinc Function [39].

The combination of wide bandwidth and a massive number of IRS elements can result in a significant reduction in array gain due to the beam-splitting effect. This combination diminishes the expected advantages of deploying IRS technology in mm-wave communications. A wide band precoding that jointly controls phase and delay is proposed to reduce the effect of beam splitting.

IV. IRS Structure Design

This paper presented a Sub-surface phase shift-TD-phase shift (PTDP) structure for IRS to mitigate hardware cost compared to the existing conventional IRS structure (Fig. 2. (a)). The IRS structure depicted in Figure 2(b) [15, 39] incorporates a TD module for each element, allowing for frequency-selective precoding. This approach effectively addresses the beam-splitting issue. However, TD modules consume more power and are more expensive to implement than phase shifters. The sub-surface delay-phase structure used for base stations in the paper [39] cannot be directly applied to IRS, as it would lead to destructive interference due to the common T.D. module. The proposed structure (Fig. 2(c)) uses two-layer phase shifters for every sub-array element linked to a shared TD. The initial phase shifter layer in the subarray creates a constructive superposition of signals. The TD module then adjusts the timing of these signals, and the second-layer phase shifter steers the resulting beam in the desired direction. The PTDP-based IRS structure was implemented using a configuration consisting of two smaller antenna patches, each equipped with two layers of phase shifters. Since low-resolution phase shifting is not limited to the traditional TD in terms of economic necessity, it reduces hardware costs and energy consumption [41].

For the IRS-assisted mm-wave technology, it was assumed that the IRS is divided into $S = S_1 S_2$ sub-arrays, where every sub-array is linked to a time-delay (T.D.) unit. Each sub-array consists of $P = P_1 P_2$ elements, where $P_1 = \frac{N_1}{S_1}$ and $P_2 = \frac{N_2}{S_2}$. The values of P_1 and P_2 were designed to be integers. For simplicity, it represented the parameter of the sub-arrays as $s_1 = 1, \dots, S_1$, and $s_2 = 1, \dots, S_2$. Similarly, the parameter of the elements within every sub-array was represented as $p_1 = 1, \dots, P_1$, and $p_2 = 1, \dots, P_2$.

After the structure was changed and divided into subarrays, the channel equations (3 and 8) must be reformulated, and the BS-IRS channel is represented as [29]:

$$G_q = \frac{g_1(f_q, d_a)}{\sqrt{N}} e^{-j2\pi f_q t_1} \underbrace{e^{j\pi m(n_1 a + n_2 \vartheta)}}_{steering\ matrix} \quad (15)$$

and the IRS-U channel is

$$V_q = \frac{g_2(f_q, d_b)}{\sqrt{N}} e^{-j2\pi f_q t_2} e^{j\pi m(n_1 a + n_2 \vartheta)} \quad (16)$$

where $a = sin\alpha cos\beta$, $\vartheta = sin\alpha sin\beta$, $n_1 = s_1 P_1 + p_1$, $n_2 = s_2 P_2 + p_2$.

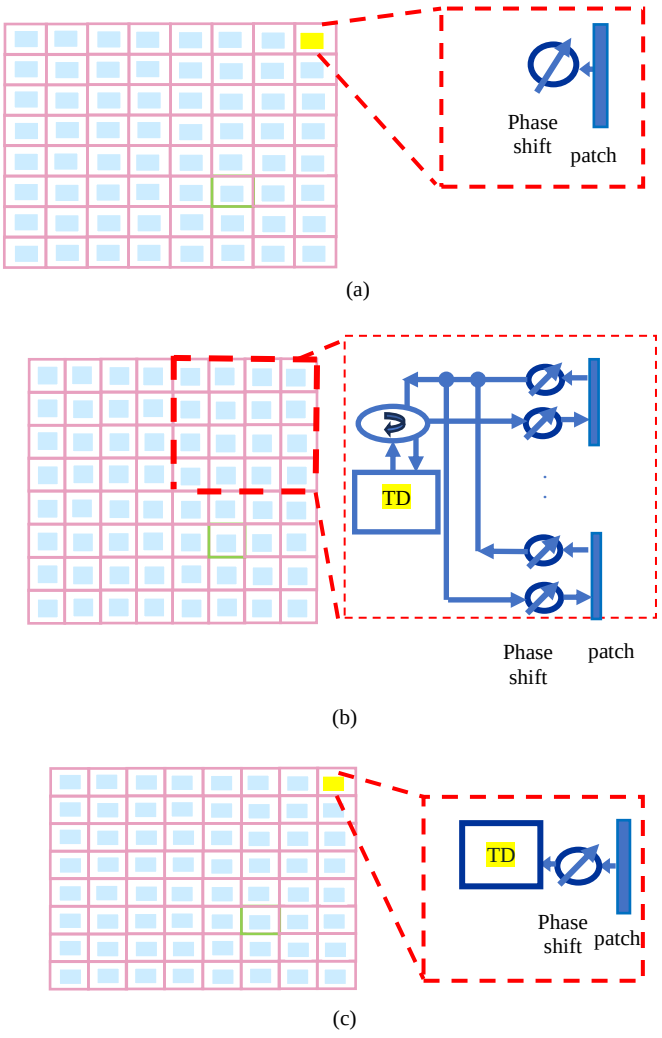

Fig. 2. The IRS Structure of: (a) The Traditional IRS (b) The TD-phase structure-based IRS (c) Proposed PTDP structure-based IRS

As defined in equations (15) and (16), the channels G_q and v_q Are partitioned into submatrices. Specifically, G_q^s Represents the channel to the s[th] sub-array of the IRS. Let TD $t_s \in \mathcal{R}^+$, ψ_1^s the phase shift in the layer 1, ψ_2^s the phase shift in layer 2 associated with the s[th] subarray, and $s = s_2 S_1 + s_1 + 1$. The TD vector (T_q) Of the IRS elements were represented as [23]:

$$T_q = e^{-j2\pi f_q t}, t = \left[t_1, t_2, \dots, t_s, \dots . t_{S_1 S_2}\right]^T \quad (17)$$

The signal received by the User after passing through the second phase-shifting layer is represented as [23]

$$y_{2,q}^s = \sum_{q=1}^{Q} (V_q^s \odot \psi_2^s T_q^s y_{1,q}^s) \quad (19)$$

Based on equations (18) and (19), the array gain of the s[th] subarray of IRS, when operating at the q[th] subcarrier, was represented by the following equation [29]:

$$\mathbb{G}_s\left(T_q^s, f_q\right) = \left|\sum_{q=1}^{Q}\left(V_q^s \odot \left[\psi_2^s T_q^s \cdot \sum_{q=1}^{Q}\left(\psi_1^s \odot G_q^s\right)\right]\right)\right| \quad (20)$$

Equation (20) forces that introducing additional TDs and phase shifts as proposed design parameters enables the presented PTDP structure to achieve high array gains across different subcarriers, thereby mitigating the effect of the beam splitting.

The performance of the PTDP-based IRS in terms of array gain was evaluated, and a novel wideband precoding technique was proposed to mitigate the detrimental effects of beam splitting. According to equation (20), the array gain of the IRS for the q[th] subcarrier was calculated [23]:

$$\mathbb{G}\left(T_q^s, f_q\right) = \left|\sum_{s_1=1}^{S_1}\sum_{s_2=1}^{S_2}\left\{\sum_{q=1}^{Q}\left(V_q^s \odot \left[\psi_2^s T_q^s \cdot \sum_{q=1}^{Q}\left(\psi_1^s \odot G_q^s\right)\right]\right)\right\}\right| \quad (21)$$

The presented wideband precoding design leverages the PTDP structure to maximize the IRS array gain, which can be formulated as [23]

$$\max_{\psi_1,\psi_2,t} \frac{1}{Q}\sum_{q=1}^{Q}\mathbb{G}\left(T_q^s, f_q\right) \quad (22)$$

The presented design of PTDP-based wideband precoding achieves better performance at q[th] subcarrier if and only if conditions (23) to (25) are met [23, 42].

$$t_s = \frac{1}{2f_c}\left[\begin{array}{l}\left((s_1-1)P_1 - \frac{(P_1-1)}{2}\right)(a_1+a_2) + \\ \left((s_2-1)P_2 - \frac{(P_2-1)}{2}\right)(\vartheta_1+\vartheta_2)\end{array}\right] \quad (23)$$

$$\psi_1^s(p_1,p_2) = e^{-j\pi(p_1a_1+p_2\vartheta_1)} \quad (24)$$

$$\psi_2^s(p_1,p_2) = e^{-j\pi(p_1a_2+p_2\vartheta_2)} \quad (25)$$

The TD (t_s), phase shift in layer 1(ψ_1^s) and phase shift in layer 2 (ψ_2^s). As equation (18) results in a scalar value, optimizing equation (22) is equivalent to independently maximizing equations (18) and (19).

The (p_1, p_2)-th element of the s[th] partitioned matrices of G_q Was represented as [23]:

$$G_{q(p_1,p_2)}^s = \frac{g_1\left(f_q, d_a\right)}{\sqrt{N}}\, e^{-j2\pi f_q t_1} e^{j\pi m(n_1a_1+n_2\vartheta_1)}$$

$$= \frac{g_1(f_q,d_a)}{\sqrt{N}}\, e^{-j2\pi f_q t_1} e^{j\pi m(s_1P_1a_1+s_2P_2\vartheta_1)} \cdot e^{j\pi m(p_1a_1+p_2\vartheta_1)} \quad (26)$$

The phase shifts for the first layer are calculated by finding the values of ψ_1^sthat maximizes the sum of the product of ψ_1^s and G_q^s Overall values of q.

The term $e^{-j2\pi f_q t_1}$ With a magnitude of 1 can be ignored, leading to the following expression [42]:

$$\sum \psi_1^s \odot G_q^s$$

$$= \frac{g_1\left(f_q, d_a\right)}{\sqrt{N}}\, e^{j\pi m(s_1P_1a_1+s_2P_2\vartheta_1)} \cdot \sum_1^{P_1}\sum_1^{P_2} e^{j\pi(m-1)(p_1a_1+p_2\vartheta_1)}$$

$$= \frac{P_1P_2g_1\left(f_q,d_a\right)}{\sqrt{N}}\, e^{j\pi m(s_1P_1a_1+s_2P_2\vartheta_1)} \cdot e^{\frac{j\pi(m-1)(P_1-1)a_1}{2}} \cdot$$

$$e^{\frac{j\pi(m-1)(P_2-1)\vartheta_1}{2}} \cdot \mathbb{F}_{P_1}\left((m-1)a_1\right) \cdot \mathbb{F}_{P_2}\left((m-1)\vartheta_1\right) \quad (27)$$

By substituting (a_1, ϑ_1) with (a_2, ϑ_2), it concluded $\psi_{1(p_1,p_2)}^s$and the sum of $(V_q^s \odot \psi_2^s)$. The normalized array gain can be calculated by substituting the derived formulas into equation (21) [29, 42].

$$\mathbb{G}\left(T_q^s, f_q\right) = \frac{P_1^2P_2^2}{N_1N_2}\left|\, \mathbb{F}_{P_1}\left((m-1)a_1\right)\mathbb{F}_{P_2}\left((m-1)a_2\right)\right.\cdot$$

$$\mathbb{F}_{P_1}\left((m-1)\vartheta_1\right)\mathbb{F}_{P_2}\left((m-1)\vartheta_2\right)$$

$$\sum_1^{S_1}\sum_1^{S_2}\left(e^{-j2\pi f_q t_s} \cdot e^{j\pi m\left[\begin{array}{l}\left((s_1-1)P_1-\frac{(P_1-1)}{2}\right)(a_1+a_2)\\ +\left((s_2-1)P_2-\frac{(P_2-1)}{2}\right)(\vartheta_1+\vartheta_2)\end{array}\right]}\right) \quad (28)$$

Equation (30) depends on f_q. To mitigate beam splitting across all subcarriers t_s It should be derived to maximize equation (30) by ensuring constructive interference and this requires satisfying [23].

$$\left(e^{-j2\pi f_q t_s} \cdot e^{j\pi m\left[\left((s_1-1)P_1-\frac{(P_1-1)}{2}\right)(a_1+a_2)+\left((s_2-1)P_2-\frac{(P_2-1)}{2}\right)(\vartheta_1+\vartheta_2)\right]}\right) = 1.$$

The value t_s Ensures accurate alignment of the beams with the desired physical direction throughout the bandwidth. In addition, ψ_1^s It can create superimposed constructive interference signals that can be received from different elements in the subarray. Furthermore, ψ_2^s It is responsible for steering the beam to the user(U) at the carrier frequency. The normalized array gain of the PTDP-based IRS $\mathbb{G}\left(T_q, f_q\right)$ Was calculated using the following equation [23]:

$$\mathbb{G}(T_q^s, f_q) = \frac{S_1S_2P_1P_2}{N}\left|\, \mathbb{F}_{P_1}\left((m-1)a_1\right)\mathbb{F}_{P_2}\left((m-1)a_2\right)\right.\cdot$$
$$\left.\mathbb{F}_{P_1}\left((m-1)\vartheta_1\right)\mathbb{F}_{P_2}\left((m-1)\vartheta_2\right)\right| \quad (29)$$

Algorithm 1 shows the steps of beamforming of PTDP. The difference between Ideal Phase Shift and PTDP Phase Shift, the first is computed directly based on the frequency and index of the IRS element. However, the second includes a delay component adjusted for sub-arrays and phase shifts from sub-array layers. Based on equation (12), the optimal beamforming vector for the IRS must vary with frequency[19]:

$$\theta_{opt,\ell} = -\pi m[n_1(a_1 + a_2) + n_2(\vartheta_1 + \vartheta_2)] \quad (30)$$

ALGORITHM 1: PROPOSED PTDP BEAMFORMING

Input: The angles (α_1),(β_1) of (AoA)of the IRS, (α_2) and (β_2) of (AoD) of the IRS,

Initialization:

1. Compute $a_1 = sin\alpha_1 cos\beta_1, \vartheta_1 = sin\alpha_1 sin\beta_1, a_2 = sin\alpha_2 cos\beta_2, \vartheta_2 = sin\alpha_2 sin\beta_2$.
2. Compute equation (23)
3. Compute the equations (24) and (25)

Output: The array gain in equation (26)

V. ANALYSIS OF DOUBLE BEAM SPLITTING EFFECT

Massive MIMO is implemented at the base station, thus showing the double beam splitting. By analyzing the gain of the array, the common wideband precoding of IRS and BS is separated to facilitate the solution. Figure 3 shows that the beams emitted from the base station are split into different directions for each subcarrier, which complicates the process of aligning them with the IRS. Additionally, the reflected and bounced beams scatter in different directions, making it difficult to accurately direct them toward the base station and the receiver. Therefore, it leads to severe double array gain loss in the IRS-assisted mm-wave communication system. From equation (10), The array gain was expressed as [23, 29]

$$\mathbb{G}(f_q) = \left|V_q^T \psi G_q w\right|$$

$$= \left|g_1(f_q, d_a) g_2(f_q, d_b)\right|.$$

$$\left|k^T(f_q, \alpha_2, \beta_2)\psi\, k(f_q, \alpha_1, \beta_1) b^H(f_q, \emptyset) w\right|$$

$$= \left|g_1(f_q, d_a) g_2(f_q, d_b)\right| \mathbb{G}_{RIS}(f_q) \mathbb{G}_{BS}(f_q) \quad (31)$$

$\mathbb{G}_{RIS}(f_q)$ and $\mathbb{G}_{BS}(f_q)$ Represented the normalized array gain of IRS and base station, respectively.

Analogous to equation (11), the normalized array gain of the BS is expressed by [23]:

$$\mathbb{G}_{BS}(f_q) = \left|b^H(f_q, \emptyset) w\right| \quad (32)$$

The joint wideband precoding problem of maximizing $\mathbb{G}(f_q)$can be decomposed into two separate optimization problems: maximizing $\mathbb{G}_{RIS}(f_q)$and maximizing $\mathbb{G}_{BS}(f_q)$. This approach allows for independent optimization of the wideband precoding at the base station and the IRS. In other words, the effect of double beam splitting was analyzed into two separate components, allowing for the decoupling of the joint wideband precoding design. This simplification does not compromise optimality. Specifically, the proposed PTDP-based wideband precoding design addresses the beam split issue at the IRS. Beam splitting at the base station (BS) can be solved in a manner akin to the wideband precoding design based on PTDP. Specifically, the Angle of Arrival and Angle of Departure of the IRS are simplified to the transmit angle of the BS (∅), and the UPA is simplified to the ULA with (B) Antennas.

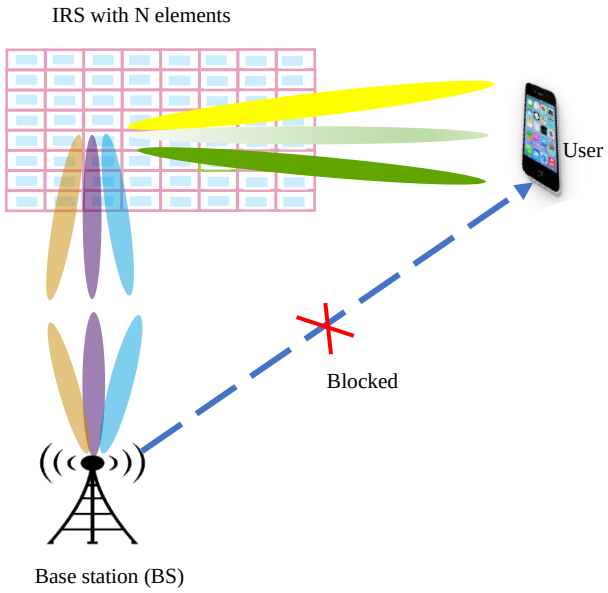

Fig. 3. Scenario of the effect of double beam splitting at BS and IRS

The base station was assumed to be divided into D subarray, and each joined to a TD unit. Define $t_D^{BS} \in \mathcal{R}^+$ the TD and $w_{u,D}$ As the matrix of phase shifting associated with the d[th] subarray at the base station. Therefore, at the q[th] subcarrier, the transmit precoding of BS was computed [23]:

$$W_q = w_u T_q^{BS} = blkdiag\left(\left[w_{u,1}, w_{u,2}, \ldots\ldots, w_{u,D}\right]\right).$$

$$e^{-j2\pi f_q}[t_1^{BS}, t_2^{BS}, \ldots\ldots, t_D^{BS}]^T \quad (33)$$

$$\left[w_{u,1}^T, w_{u,2}^T, \ldots\ldots, w_{u,D}^T\right]^T = b(f_c, \emptyset) \quad (34)$$

The steering vector of the ULA is denoted by b in equation (7). The steps of the proposed PTDP-based wideband precoding algorithm were provided in Algorithm 2.

ALGORITHM 2: PROPOSED PTDP-BASED WIDEBAND PRECODING

Input: The angles (α_1),(β_1) of (AoA)of the IRS, (α_2), (β_2) of (AoD) of the IRS, and the angle at BS (∅)

Initialization:

1. Compute $a_1 = sin\alpha_1 cos\beta_1, \vartheta_1 = sin\alpha_1 sin\beta_1, a_2 = sin\alpha_2 cos\beta_2, \vartheta_2 = sin\alpha_2 sin\beta_2$.
2. Compute the TD(t_s).
3. Compute the phase shifts (ψ_1^s) and (ψ_2^s)

Output: Compute BS transmit precoding W_q

VI. RESULTS OF SIMULATION

The IRS-assisted millimetre wave communication system described in Sections III and IV and shown in Figure 1 was

simulated using the specified parameters shown in Table I. The channel state information (CSI) is assumed to be completely known [11], which is obtained using the algorithms mentioned in [13, 14].

TABLE I
PROPOSED PARAMETERS IN THE SIMULATION

Parameter	Definition	Value
d_a	Distance between BS and IRS	*25m*
d_b	Distance between the IRS and the user	*25m*
N	Number of IRS elements ($N_1 \times N_2$)	*64×64*
S	sub-arrays in IRS	*16 ×16*
Q	Number of subcarriers	*128*
f_c	Carrier frequency	*28GHz*
f_s	Bandwidth	*2GHz*
B	Number of antennas at BS	*1*
α_1	The elevation angle of (AoA)of the IRS	$\frac{\pi}{4}$
β_1	The azimuth angle of (AoA)of the IRS	$\frac{\pi}{2}$
α_2	The elevation angle of (AoD)	$\frac{\pi}{4}$
β_2	The azimuth angle of (AoD)	0

A fixed elevation angle and a fixed azimuth angle are defined, which represent a specific physical direction where the array gain reaches its maximum. Figure 4 shows, in a 2D representation, the relationship between the array gain and the elevation and azimuth angles separately. The beam produced at the carrier frequency fc was used as a reference for comparison and then compared to the beams produced at other frequencies ($f_{b_1}$and f_{b_2}). It was found that the beams at the edges of the band deviate significantly from the desired direction.

Figure 5 shows how the array gain changes when it changes the frequency of the subcarriers. Increasing the number of frequencies used also leads to a loss in matrix gain. As a result, a large increase in bandwidth results in a significant loss of gain, which reduces the benefits of using IRS technology. Figure 6 shows the relationship of the normalized array gain for different numbers elements of IRS. The more elements of IRS there are, the more loss there is in the array gain. Figure 7 clearly demonstrates the ability of the proposed PTDP system to direct beams generated at various frequencies with high accuracy. Unlike the previous system, which suffers from significant gain loss, the proposed system shows significant improvement in beam alignment with target angles, which confirms the effectiveness of T.D. modules and phase shifters in this system.

Figure 8 illustrates the normalized array gain at various subcarriers. Compared to Figure 5, it becomes evident that the proposed PTDP and corresponding wideband precoding design effectively alleviate the beam-splitting effect. Specifically, the normalized array gain experiences a substantial reduction of over 82% at subcarrier Q = 1 when using a narrowband of B = 0.01 GHz. The results of Figure 8 confirm the effectiveness of the proposed PTDP system in overcoming the challenge of beam splitting in IRS systems. By comparing the performance of the proposed system with the traditional system at different frequency bands, it is clear that the proposed system achieves a significant improvement in array gain, especially at wide bands. The proposed design achieved a 94.5% improvement in gain compared to the traditional approach. Figure 9 shows the relationship between the transmission power of the base station and the achievable rate of each subcarrier.

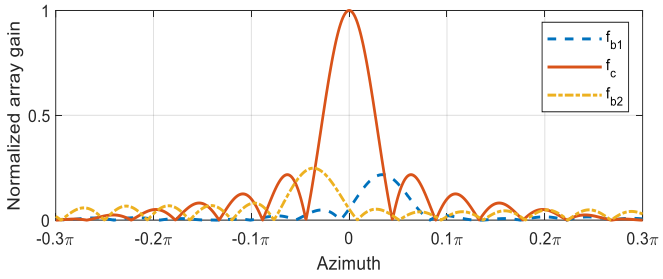

(a)

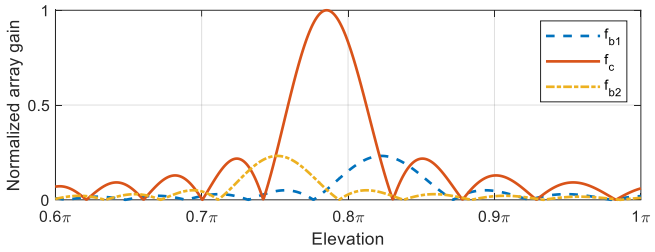

(b)

Fig. 4. The normalized array gain against (a) Azimuth angle and (b) Elevation angle

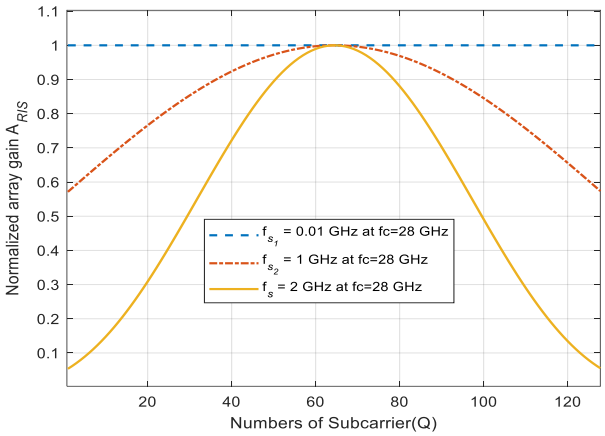

Fig. 5. The relationship between normalized array gain and no. sub-carrier for bandwidths $f_{s1} = 0.01\ GHz, f_{s1} = 1\ GHz, and\ f_{s1} = 2\ GHz.$

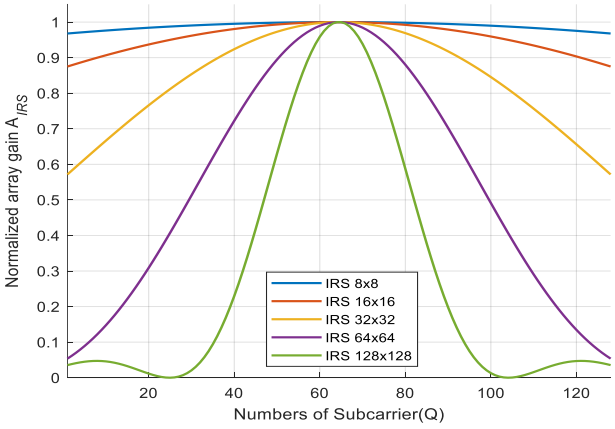

Fig. 6. The relationship between normalized array gain and no. sub-carrier for different numbers elements of IRS

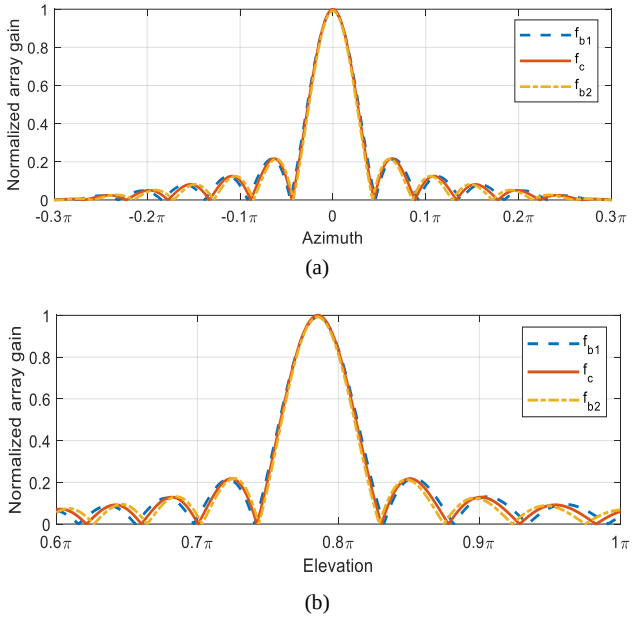

(a)

(b)

Fig.7. The normalized array gain against (a) Azimuth angle and (b)Elevation angle using proposed PTDP

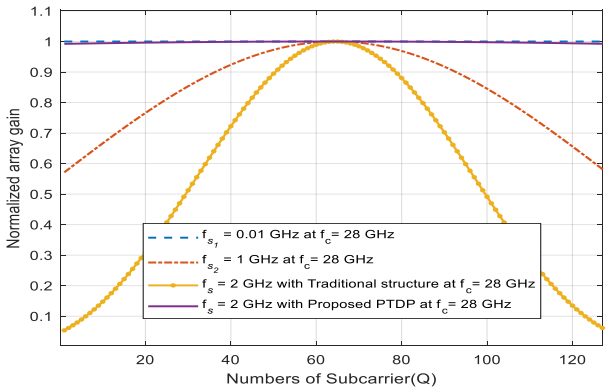

Fig. 8. The relationship between the number of sub-carriers and normalized array gain using the proposed PTDP structure

It is shown that the proposed system, with its frequency-based precoding design, achieves the highest possible performance when each element is equipped with a TD. The design was based on traditional narrowband beamforming technology, with an emphasis on improving phase control performance. The performance of this technique was evaluated using continuous phase shifting and phase shifting at low resolutions (1 and 2 bits), compared to the traditional technique. The proposed design was also matched with the optimal precoding. Traditional narrowband beamforming design has been based on simple phase shift techniques. The proposed PTDP system relied on more complex phase-shifting techniques, which allowed for significant performance improvement. The results showed that using TD in Phase shift-Time Delay-Phase delay (PTDP)resulted in a 54% increase at transmitted power=30 dBm in data rate compared to the traditional design. The achievable rate per subcarrier is given [43, 44]:

$$R_{optimal} = \frac{1}{Q}\sum_{q=1}^{Q} log_2\left(1+\frac{|G_q|^2.SNR}{\sigma^2}\right) \quad (35)$$

The signal-to-noise ratio is [45]:

$$SNR = P_t/\sigma^2 \quad (36)$$

where P_t is the total transmitted power, while $\sigma^2 = -90dBm$ [11, 46]. The achievable rate for continuous precoding is given [23] :

$$R_{con} = \frac{1}{Q}\sum_{q=1}^{Q} log_2\left(1+\frac{|\psi_1 G_q \psi_2|^2 SNR}{\sigma^2}\right) \quad (37)$$

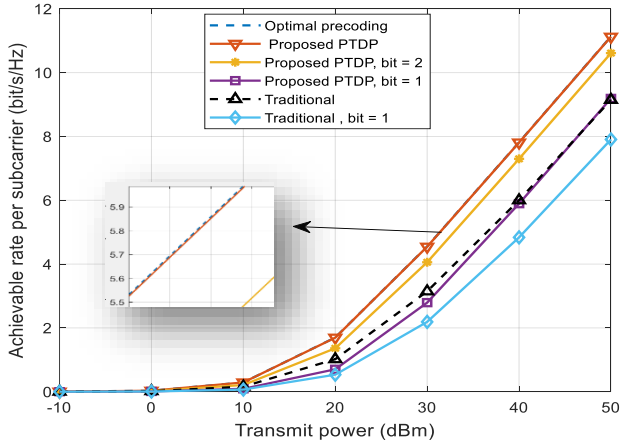

Fig. 9. The relationship between the transmitted power and achievable rate per subcarrier at the number of BS antennas B=1

Figure 10 shows that as the number of subarrays increases, this leads to an increase achievable rate per subcarrier and its value approaches the optimal precoding. Figure (11) shows the relationship between the transmitted power and the achievable rate of each sub-carrier when the number of base station antennas is B=256 antenna, and the RIS uses 16-TD units. Each simulation randomly selected the base station transmission angle from a uniform distribution between -π/2 and π/2. The performance of a PTDP-based wideband precoding scheme, which used continuous phase shift and 256 RIS subarray, was analyzed.

An optimal precoding design was adopted for both the base station and the IRS to achieve maximum performance. A narrowband beamforming design without TD modules was considered a baseline for comparison. This baseline scenario provides an example of the double beam splitting phenomenon. For comparison, the performance of TD-based precoding that is limited to beam splitting processing in either IRS or BS. only, based on a proposed design, was also evaluated. Compared with single-antenna base stations, multi-antenna base stations with large antennas suffer greater data rate degradation due to the double beam split phenomenon when using a narrowband beamforming design.

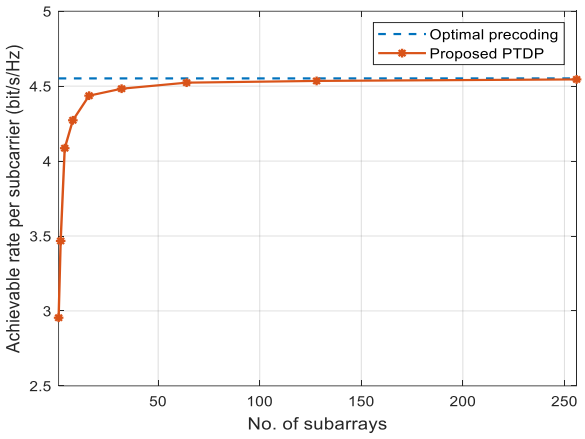

Fig. 10. The relationship between the number of subarrays and the achievable rate per subcarrier

While TD modules-based precoding can help address the beam-splitting effect, focusing on only the BS or the IRS does not fully compensate for the performance degradation caused by double beam splitting. The PTDP-based joint wideband precoding design is able to enhance a performance that is close to the optimal achievable rate, and this is particularly effective in mitigating the double beam splitting effect. Figure (12) The relationship between the transmitted power and achievable rate per subcarrier at the number of BS antennas B=256. The results showed that both the PTDP design with a 16-TD and the conventional narrow-beamforming technique led to lower-than-expected performance when operating in narrow frequency bands. In contrast to the proposed PTDP-based design, the frequency-independent narrowband beamforming scheme experiences a significant decrease in achievable rate as the bandwidth increases.

The proposed PTDP-based wideband precoding design is shown to be able to effectively handle the challenge of dual beam splitting in wide frequency bands and this makes it a flexible and applicable solution in IRS-based millimetre wave communication systems.

Finally, the proposed method was compared with a number of other methods in Table II.

TABLE II
COMPRESSION BETWEEN THE PROPOSED PAPER WITH NUMBERS OF PAPERS

	[19]	[44]	[47]	[29]	The proposed
Single user	✓			✓	✓
Multi-user		✓	✓		✓
Narrowband					✓
Wideband	✓	✓	✓	✓	✓
Beam Squint	✓		✓		✓
Beam spilt		✓		✓	✓
With IRS		✓	✓	✓	✓

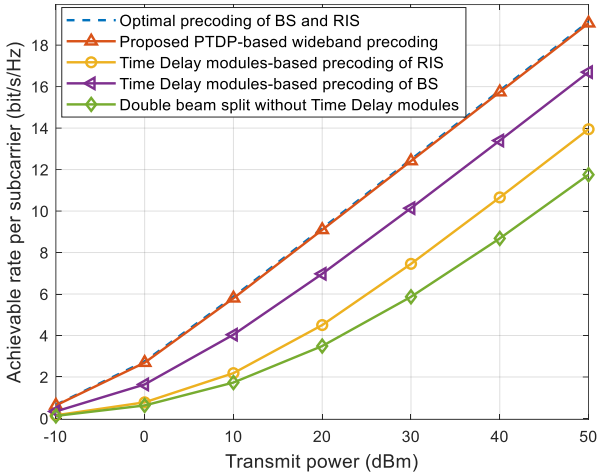

Fig. 11. The relationship between the transmitted power and achievable rate per subcarrier at the number of BS antennas B=256.

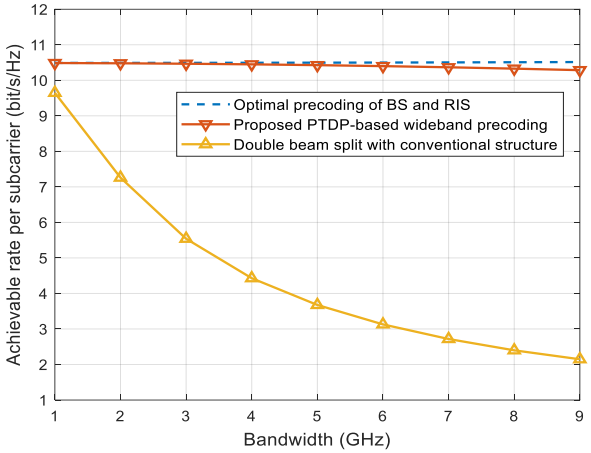

Fig. 12. The relationship between Bandwidth and achievable rate per subcarrier at the number of BS antennas B=256 and the transmitted power=30dBm.

VII. CONCLUSION

Millimetre wave communications supported by IRS have faced the major challenge of beam splitting, resulting in a decrease in received signal strength, while to solve this problem, precoding techniques based on phase control and TD of the signal have been studied. By analyzing the effect of beam splitting and gain drop, a structure of IRS consisting of several interconnected layers is presented. This structure allows the application of a frequency-based and error-tolerant precoding technique in estimating communication channels. The effect of double beam splitting at both BS and RIS is studied. The results show that this technology can significantly reduce the effect of beam splitting, making IRS-supported millimetre wave technology more efficient. The proposed PTDP structure achieved a 94.5% enhancement in gain compared to the traditional structure. The proposed PTDP-based wideband precoding design has been demonstrated to be able to compensate for the array gain loss caused by the double beam splitting effect occurring at both BS and IRS, even in scenarios with large bandwidths.

REFERENCES

[1] I. P. Roberts, Y. Zhang, T. Osman, and A. Alkhateeb, "Real-World Evaluation of Full-Duplex Millimeter Wave Communication Systems," *IEEE Transactions on Wireless Communications,* 2024. doi: 10.1109/TWC.2024.3376298

[2] B. M. Ahmad, F. E. Mahmood, and H. A. Alsawaf, "Non Orthogonal Multiple Access verses Orthogonal Multiple Access performance comparison in 5G communication systems," *Przeglad Elektrotechniczny,* vol. 99, 2023. doi:10.15199/48.2023.01.25

[3] R. A. Abed and S. A. Ayoob, "Millimeter wave beams coordination and antenna array height effect," in *AIP Conference Proceedings*, 2023. https://doi.org/10.1063/5.0157290

[4] S. A. Ahmed, S. A. Ayoob, and A. O. Al Janaby, "On the performance of multi-user massive MIMO over mm wave channels," in *2021 7th International Conference on Contemporary Information Technology and Mathematics (ICCITM)*, 2021, pp. 100-105. doi: 10.1109/ICCITM 53167.2021.9677730.

[5] F. S. Alsharbaty and S. A. Ayoob, "Intra-site CoMP operation effect of fifth generation techniques on 802.16 e downlink stream," *International Journal of Engineering Trends and Technology,* vol. 67, pp. 12-17, 2019. doi:10.14445/22315381/IJETT-V67I4P204.

[6] S. A. Ayoob, F. S. Alsharbaty, and A. Alhafid, "Enhancement the heavy file application of 802.16 e cell using intra-site CoMP in uplink stream," *Journal of Engineering Science and Technology,* vol. 17, pp. 1721-1733, 2022.

[7] Q. Wu and R. Zhang, "Towards smart and reconfigurable environment: Intelligent reflecting surface aided wireless network," *IEEE communications magazine,* vol. 58, pp. 106-112, 2019. doi:10.1109/MCOM.001.1900107

[8] R. Li, B. Guo, M. Tao, Y.-F. Liu, and W. Yu, "Joint design of hybrid beamforming and reflection coefficients in RIS-aided mmWave MIMO systems," *IEEE Transactions on Communications,* vol. 70, pp. 2404-2416, 2022. doi:10.1109/TCOMM.2022.3144986

[9] Z. Zhang and L. Dai, "A joint precoding framework for wideband reconfigurable intelligent surface-aided cell-free network," *IEEE Transactions on Signal Processing,* vol. 69, pp. 4085-4101, 2021. doi:10.1109/TSP.2021.3088755

[10] B. J. Qeryaqos and S. A. Ayoob, "Optimizing the Signal-to-Noise Ratio using the Virtual Line of Sight and choosing the appropriate dimensions," *International Journal of Electronics and Telecommunication,* vol. 70, pp. 909-914, 2024. doi: 10.24425/ijet.2024.152077

[11] P. Wang, J. Fang, X. Yuan, Z. Chen, and H. Li, "Intelligent reflecting surface-assisted millimeter wave communications: Joint active and passive precoding design," *IEEE Transactions on Vehicular Technology,* vol. 69, pp. 14960-14973, 2020. doi:10.1109/TVT.2020.3031657.

[12] B. J. Qeryaqos and S. A. Ayoob, "Proposed Multiple Reconfigurable Intelligent Surfaces to Mitigate the Inter-User-Interference Problem in NLOS.", *Journal of Communications Software and Systems*,vol.20, pp. 245-252, 2024, doi: 10.24138/jcomss-2024-0039.

[13] S. Ma, W. Shen, J. An, and L. Hanzo, "Wideband channel estimation for IRS-aided systems in the face of beam squint," *IEEE Transactions on Wireless Communications,* vol. 20, pp. 6240-6253, 2021. doi:10.1109/TWC.2021.3072694

[14] C. Hu, L. Dai, S. Han, and X. Wang, "Two-timescale channel estimation for reconfigurable intelligent surface aided wireless communications," *IEEE Transactions on Communications,* vol. 69, pp. 7736-7747, 2021. doi: 10.1109/TCOMM.2021.3072729

[15] K. Liu, Z. Zhang, L. Dai, S. Xu, and F. Yang, "Active reconfigurable intelligent surface: Fully-connected or sub-connected?," *IEEE Communications Letters,* vol. 26, pp. 167-171, 2021. doi:10.1109/LCOMM.2021.3119696

[16] C. Pan, H. Ren, K. Wang, W. Xu, M. Elkashlan, A. Nallanathan*, et al.*, "Multicell MIMO communications relying on intelligent reflecting surfaces," *IEEE Transactions on Wireless Communications,* vol. 19, pp. 5218-5233, 2020. doi:10.1109/TWC.2020.2990766.

[17] M. He, W. Xu, H. Shen, G. Xie, C. Zhao, and M. Di Renzo, "Cooperative multi-RIS communications for wideband mmWave MISO-OFDM systems," *IEEE Wireless Communications Letters,* vol. 10, pp. 2360-2364, 2021. doi:10.1109/LWC.2021.3100479

[18] P. Wang, J. Fang, W. Zhang, and H. Li, "Fast beam training and alignment for IRS-assisted millimeter wave/terahertz systems," *IEEE Transactions on Wireless Communications,* vol. 21, pp. 2710-2724, 2021. doi: 10.1109/TWC.2021.3115152.

[19] Y. Chen, D. Chen, and T. Jiang, "Beam-squint mitigating in reconfigurable intelligent surface aided wideband mmWave communications," in *2021 IEEE Wireless Communications and Networking Conference (WCNC)*, 2021, pp. 1-6. doi:10.1109/WCNC49053.2021.9417413.

[20] P. Nuti, E. Balti, and B. L. Evans, "Spectral efficiency optimization for mmWave wideband MIMO RIS-assisted communication," in *2022 IEEE 95th Vehicular Technology Conference:(VTC2022-Spring)*, 2022, pp. 1-6. doi:10.1109/VTC2022-Spring54318.2022.9860779.

[21] R. Wang, Y. Yang, B. Makki, and A. Shamim, "A wideband reconfigurable intelligent surface for 5G millimeter-wave applications," *IEEE transactions on antennas and propagation,* 2024. doi: 10.1109/TAP.2024.3352828.

[22] Y. Zhao, X. Liu, H. Liu, X. Wang, and L. Huang, "RIS-Aided MmWave Hybrid Relay Network Based on Multi-Agent Deep Reinforcement Learning," *Mobile Networks and Applications,* pp. 1-16, 2024. doi: 10.21203/rs.3.rs-3834169/v1.

[23] L. Dai, J. Tan, Z. Chen, and H. V. Poor, "Delay-phase precoding for wideband THz massive MIMO," *IEEE Transactions on Wireless Communications,* vol. 21, pp. 7271-7286, 2022. doi: 10.1109/TWC.2022.3157315.

[24] Y. Chen, Y. Xiong, D. Chen, T. Jiang, S. X. Ng, and L. Hanzo, "Hybrid precoding for wideband millimeter wave MIMO systems in the face of beam squint," *IEEE transactions on wireless communications,* vol. 20, pp. 1847-1860, 2020. doi: 10.1109/TWC.2020.3036945.

[25] J. An, C. Xu, D. W. K. Ng, C. Yuen, L. Gan, and L. Hanzo, "Reconfigurable intelligent surface-enhanced OFDM communications via delay adjustable metasurface," *arXiv preprint arXiv:2110.09291,* 2021. doi: 10.48550/arXiv.2110.09291.

[26] S.-H. Park, B. Kim, D. K. Kim, L. Dai, K.-K. Wong, and C.-B. Chae, "Beam squint in ultra-wideband mmWave systems: RF lens array vs. phase-shifter-based array," *IEEE Wireless Communications,* vol. 30, pp. 82-89, 2022. doi: 10.1109/MWC.007.2100530.

[27] A. Abdallah, A. Celik, M. M. Mansour, and A. M. Eltawil, "Deep-learning based channel estimation for RIS-aided mmWave systems with beam squint," in *ICC 2022-IEEE International Conference on Communications*, 2022, pp. 1269-1275. doi: 10.1109/ICC45855.2022.9839142

[28] R. Li, X. Shao, S. Sun, M. Tao, and R. Zhang, "IRS Aided Millimeter-Wave Sensing and Communication: Beam Scanning, Beam Splitting, and Performance Analysis," *arXiv preprint arXiv:2401.15344,* 2024. doi: 10.1109/TWC.2024.3486023.

[29] W. Yan, W. Hao, G. Sun, C. Huang, and Q. Wu, "Wideband beamforming for Star-RIS-assisted THZ communications with three-side beam split," *IEEE Transactions on Communications,* 2024. doi: 10.1109/TCOMM. 2024.3464412.

[30] G. Torcolacci, A. Guerra, H. Zhang, F. Guidi, Q. Yang, Y. C. Eldar*, et al.*, "Holographic imaging with XL-MIMO and RIS: Illumination and reflection design," *IEEE Journal of Selected Topics in Signal Processing,* 2024. doi: 10.1109/JSTSP.2024.3417356.

[31] Y. Xiu, J. Zhao, W. Sun, M. Di Renzo, G. Gui, Z. Zhang*, et al.*, "Reconfigurable intelligent surfaces aided mmWave NOMA: Joint power allocation, phase shifts, and hybrid beamforming optimization," *IEEE Transactions on Wireless Communications,* vol. 20, pp. 8393-8409, 2021. doi: 10.48550/arXiv.2007.05873.

[32] M. Di Renzo, A. Zappone, M. Debbah, M.-S. Alouini, C. Yuen, J. De Rosny*, et al.*, "Smart radio environments empowered by reconfigurable intelligent surfaces: How it works, state of research, and the road ahead," *IEEE journal on selected areas in communications,* vol. 38, pp. 2450-2525, 2020. doi: 10.1109/JSAC.2020.3007211.

[33] B. Ning, Z. Chen, W. Chen, Y. Du, and J. Fang, "Terahertz multi-user massive MIMO with intelligent reflecting surface: Beam training and hybrid beamforming," *IEEE Transactions on Vehicular Technology,* vol. 70, pp. 1376-1393, 2021. doi: 10.1109/TVT.2021.3052074.

[34] Y. Liu, S. Zhang, F. Gao, J. Tang, and O. A. Dobre, "Cascaded channel estimation for RIS assisted mmWave MIMO transmissions," *IEEE Wireless Communications Letters,* vol. 10, pp. 2065-2069, 2021.doi: 10.1109/LWC.2021.3092147.

[35] W. Mei and R. Zhang, "Multi-beam multi-hop routing for intelligent reflecting surfaces aided massive MIMO," *IEEE Transactions on Wireless Communications,* vol. 21, pp. 1897-1912, 2021. doi: 10.1109/TWC. 2021.3108020.

[36] R. Li, S. Sun, and M. Tao, "Ergodic achievable rate maximization of RIS-assisted millimeter-wave MIMO-OFDM communication systems," *IEEE Transactions on Wireless Communications,* vol. 22, pp. 2171-2184, 2022. doi: 10.1109/TWC.2022.3210227.

[37] T. Ling, Y. Han, S. Jin, and M. Matthaiou, "Two-phase parameter-based separate channel estimation in RIS-Aided MIMO OFDM systems," in *ICC 2023-IEEE International Conference on Communications*, 2023, pp. 4329-4334. doi: 10.1109/ICC45041.2023.10278782.

[38] X. Pei, H. Yin, L. Tan, L. Cao, Z. Li, K. Wang*, et al.*, "RIS-aided wireless communications: Prototyping, adaptive beamforming, and indoor/outdoor field trials," *IEEE Transactions on Communications,* vol. 69, pp. 8627-8640, 2021. doi: 10.1109/TCOMM.2021.3116151.

[39] J. Tan and L. Dai, "Delay-phase precoding for THz massive MIMO with beam split," in *2019 IEEE Global Communications Conference (GLOBECOM)*, 2019, pp. 1-6. doi: 10.1109/GLOBECOM 38437.2019.9014304.

[40] Y. Wei, M.-M. Zhao, M.-J. Zhao, and Y. Cai, "Channel estimation for IRS-aided multiuser communications with reduced error propagation," *IEEE Transactions on Wireless Communications,* vol. 21, pp. 2725-2741, 2021. doi: 10.1109/TWC.2021.3115161.

[41] C. Huang, G. C. Alexandropoulos, A. Zappone, M. Debbah, and C. Yuen, "Energy efficient multi-user MISO communication using low resolution large intelligent surfaces," in *2018 IEEE Globecom Workshops (GC Wkshps)*, 2018, pp. 1-6. doi: 10.1109/GLOCOMW.2018.8644519.

[42] Y. Jiang, Z. Zhou, X. Li, and Y. Gong, "Beamforming Design for RIS-Aided THz Wideband Communication Systems," in *2023 IEEE 24th International Workshop on Signal Processing Advances in Wireless Communications (SPAWC)*, 2023, pp. 296-300. doi: 10.1109/SPAWC 53906.2023.10304432.

[43] Y. Cheng, C. Huang, W. Peng, M. Debbah, L. Hanzo, and C. Yuen, "Achievable rate optimization of the RIS-aided near-field wideband uplink," *IEEE Transactions on Wireless Communications,* 2023. doi: 10.1109/TWC.2023.3297396.

[44] J. Wang, J. Xiao, Y. Zou, W. Xie, and Y. Liu, "Wideband Beamforming for RIS Assisted Near-Field Communications," *arXiv preprint arXiv:2401.11141,* 2024. doi: 10.1109/TWC.2024.3447570.

[45] T. Mir, M. Waqas, S. Tu, C. Fang, W. Ni, R. MacKenzie*, et al.*, "Relay hybrid precoding in uav-assisted wideband millimeter-wave massive mimo system," *IEEE Transactions on Wireless Communications,* vol. 21, pp. 7040-7054, 2022. doi: 10.1109/TWC.2022.3154290.

[46] S. Yang, C. Xie, W. Lyu, B. Ning, Z. Zhang, and C. Yuen, "Near-field channel estimation for extremely large-scale reconfigurable intelligent surface (XL-RIS)-aided wideband mmwave systems," *IEEE Journal on Selected Areas in Communications,* 2024. https://doi.org/10.1109/JSAC.2024.338912

[47] X. Mo, L. Gui, K. Ying, X. Sang, and X. Diao, "Low complexity joint hybrid precoding for RIS-assisted wideband wireless systems," *Digital Signal Processing,* vol. 140, p. 104138, 2023. doi: 10.1016/j.dsp.2023.104138.

Hiba A. Alsawaf earned her B.E. in electrical engineering/electronic and communications engineering from the University of Mosul, Iraq. The same university also awarded her a master's degree in electronic and communication engineering, and she is now working on a PhD in 6G communication and Intelligent Reflecting Surfaces. She has taught at Nineveh University's College of Electronics Engineering for 14 years. She can be contacted at emails: hiba.hmdoon@uoninevah.edu.iqand hiba.22enp24@student.uomosul.edu.iq.

Saad A. Ayoob was born in Ninevah Province, Iraq, in 1972. He received his B.E. degree from the University of Mosul, Iraq, in 1996 and his M.S. degree and Ph.D. from the same University in 2005 and 2011 respectively, both in Communication Engineering. He is currently an Assistant Prof. in the Department of Electrical Engineering University of Mosul. His research interests include networking, millimeter-wave, 5G, 6G, microstrip patch antenna, reflective intelligent surfaces (RIS), and communication systems. He can be contacted at email: sa_ah_ay@uomosul.edu.iq.